Suitability of strontium and cobalt-free perovskite cathodes with $La_{9.67}Si_5AlO_{26}$ apatite electrolyte for intermediate temperature solid oxide fuel cells

Robles-Fernandez, Adrian ; Orera, Alodia; Merino, Rosa Isabel; Slater, Peter

DOI:
10.1039/D0DT02987D

Document Version
Peer reviewed version

Citation for published version (Harvard):
Robles-Fernandez, A, Orera, A, Merino, RI & Slater, P 2020, 'Suitability of strontium and cobalt-free perovskite cathodes with $La_{9.67}Si_5AlO_{26}$ apatite electrolyte for intermediate temperature solid oxide fuel cells', *Dalton Transactions*, vol. 49, no. 40, pp. 14280–14289. https://doi.org/10.1039/D0DT02987D

Suitability of strontium and cobalt-free perovskite cathodes with $La_{9.67}Si_5AlO_{26}$ apatite electrolyte for intermediate temperature solid oxide fuel cells

Received 00th January 20xx,
Accepted 00th January 20xx

DOI: 10.1039/x0xx00000x

Adrian Robles-Fernandez [a], Alodia Orera * [a], Rosa I. Merino [a] and Peter R. Slater [b]

Aluminium-doped lanthanum silicate (LSAO) apatite-type compounds have been considered as promising candidates for substituting yttria-stabilized zirconia (YSZ) as electrolytes for intermediate temperature solid oxide fuel cells (IT-SOFC). Nevertheless, not many materials have been reported to work as cathodes in a LSAO apatite-based cell. In the present work, eight different strontium and cobalt-free compounds with a perovskite-type structure and the general composition $LaM_{1-x}N_xO_{3-\delta}$ (where M = Fe, Cr, Mn; N = Cu, Ni; and x = 0.2, 0.3) have been tested. This study includes the synthesis and structural characterization of the compounds, as well as thermomechanical and chemical compatibility tests between them. Functional characterization of the individual components has been performed by electrochemical impedance spectroscopy (EIS). Apatite/perovskite symmetrical cells were used to measure area-specific resistance (ASR) of the half cell in an intermediate temperature range (500-850°C) both with and without DC bias. According to its electrochemical behaviour, $LaFe_{0.8}Cu_{0.2}O_{3-\delta}$ is the most promising material for IT-SOFC among the compositions tested since its ASR is similar to that of traditional $(La_xSr_{1-x})MnO_3$ (LSM) cathode.

Introduction

Solid oxide fuel cells (SOFC) are well-known electrochemical devices that transform the chemical energy of a fuel into electricity via a redox reaction in which electrons are generated. This reaction involves oxygen reduction into oxide ions, which are formed in the porous cathode, then transported through a dense electrolyte, arriving at the anode where they react with the fuel, liberating electrons and closing the circuit. SOFC devices are efficient and environmentally friendly –when using hydrogen as fuel, the only residue is water– but high operation temperatures (around 1000°C) lead to degradation of components and lower long term stability of the cell.

Among the latest trends seeking an improvement on SOFC technology, reducing operation temperature from 1000°C to 600°C-800°C (intermediate temperatures, IT) is one of the most popular ones.[1,2] The key issue in this research field is finding an electrolyte with higher ionic conductivity at IT than traditional YSZ. Lanthanum silicates with the apatite structure satisfy that requirement, as Nakayama et al. first reported.[3,4] The properties of these compounds have been widely studied.[5–7] It has been also proved that doping with moderate quantities of lower valence cations both in the lanthanum and the silicon sites enhances ionic conductivity.[8–12] Al^{3+} doping at the Si-site can enhance ionic conductivities to values as high as 0.018 $S{\cdot}cm^{-1}$ at 800°C through better sintering of the compounds.[11,13–15] For this reason, $La_{9.67}Si_5AlO_{26}$ was chosen as electrolyte for an IT-SOFC in this work. On the other hand, traditional cathodes –such as $La_xSr_{1-x}MnO_3$ (LSM) or $La_xSr_{1-x}Co_yFe_{1-y}O_3$ (LSCF)– face some issues, like low ionic conductivity and high polarization losses at intermediate temperatures.[16,17]

[a] Instituto de Nanociencia y Materiales de Aragón (INMA), CSIC-Universidad de Zaragoza, 50009 Zaragoza, Spain.
[b] School of Chemistry, University of Birmingham, Birmingham, B15 2TT, UK

Besides, the strontium content has been reported to segregate towards interfaces in the SOFC,[18,19] creating Sr-rich isolating phases which downgrade the overall performance of the cell, both in thin-film[20–23] and in bulk electrodes.[24,25] The cobalt content has also been reported as detrimental for a cathode due to thermal mismatch with the electrolyte materials, which causes thermal internal stresses and may lead to delamination of the cathode/electrolyte interface.[2,26–29] Despite their high electronic conductivity, the high thermal expansion coefficients of these Co-containing compounds limit their use to composite cathodes.[30]

Table 1 compiles the area specific electrode polarization reported in the literature with different oxygen electrodes on lanthanum silicate apatite electrolyte.[31–41] The strategy followed in this work consisted of avoiding Sr and Co content, starting with some well-known compounds with the perovskite structure, such as $LaMnO_3$, $LaFeO_3$ and $LaCrO_3$ and substituting the cation in the B-site with a lower valence transition metal cation, such as Cu^{2+} or Ni^{2+}, which would increase its conductivity due to the creation of either charge balancing mixed valence and/or oxygen vacancies $\mathbf{V_O^{\cdot\cdot}}$.[29] Thus, the eight compositions summarized in table 2 will be tested as cathodes in combination with the apatite electrolyte.

Although some studies have already been reported on related manganite, ferrite and chromite compounds, as $LaMn_{1-x}Ni_xO_{3-\delta}$, $LaFe_{1-x}Ni_xO_{3-\delta}$, $LaCr_{1-x}Ni_xO_{3-\delta}$ [42,43] or $LaFe_{0.8}Cu_{0.2}O_{3-\delta}$, [44] none of these have been tested as cathodes in cells in combination with an apatite electrolyte. The aim of this work is to examine if these compounds satisfy the requirements for acting as cathodes with this electrolyte, including high electronic conductivity, chemical stability in operation conditions, and compatibility with the apatite, both chemical and thermomechanical.[45] Apatite-perovskite half cells will be manufactured and then electrochemically tested to identify the most promising cathode materials among the ones proposed.

Table 1. Previous studies on electrochemical performance of cells using an apatite electrolyte and different cathode compositions (R-P, Ruddlesden-Popper; P, perovskite; PC, pyrochlore)

Cathode Composition	Structure	Electrolyte	ASR at 800°C (Ω·cm²)	Ref.
$La_4Ni_3O_{10}$	R-P	$La_{10}Si_5AlO_{26.5}$	2.2	31
$La_4Ni_3Cu_{0.1}O_{10}$	R-P		1.6	
$La_{3.95}Sr_{0.05}Ni_2CoO_{10}$	R-P		2.7	
$La_2Ni_{0.5}Cu_{0.5}O_4$	R-P		2.2	
$La_2Ni_{0.8}Cu_{0.2}O_4$	R-P		1.5	
$Sr_{0.7}Ce_{0.3}Mn_{0.9}Cr_{0.1}O_3$	P		10.2	
$SrMn_{0.6}Nb_{0.4}O_3$	P		31	
$Gd_{0.6}Ca_{0.4}Mn_{0.9}Ni_{0.1}O_3$	P		20	
$LaSr_2Mn_{1.6}Ni_{0.4}O_7$	PC		24	
$La_2Ni_{0.8}Cu_{0.2}O_4$	R-P	$La_{10}Si_5AlO_{26.5}$	1.5	32
$La_2Ni_{0.8}Cu_{0.2}O_4$-PrO_x	R-P		0.4	
$La_2Ni_{0.8}Cu_{0.2}O_4$-Ag	R-P		0.6	
$La_{0.8}Sr_{0.2}Fe_{0.8}Co_{0.2}O_3$-GDC	P		7.2	
$La_{0.7}Sr_{0.3}MnO_3$-GDC	P		5.5	
$La_{0.6}Sr_{0.4}CoO_3$	P	$La_{10}Si_{5.8}Al_{0.2}O_{26.9}$	1.8	33
$La_{0.6}Sr_{0.4}Co_{0.8}Fe_{0.2}O_3$	P		0.3	
$La_{0.6}Sr_{0.4}Co_{0.2}Fe_{0.8}O_3$	P		1.3	
$La_{0.6}Sr_{0.4}FeO_3$	P		4.3	
$La_{0.75}Sr_{0.25}Mn_{0.8}Co_{0.2}O_3$-LSSO	P	$La_9SrSi_6O_{26.5}$	31 (700°C)	34
$La_{0.8}Sr_{0.2}Ni_{0.4}Fe_{0.6}O_3$	P	$La_{9.83}Si_5Al_{0.75}Fe_{0.25}O_{26}$	14.5	35
Nd_2NiO_4	R-P	$La_{10}Si_6O_{27}$	7 (850°C)	36
Pr_2NiO_4	R-P		2.5 (850°C)	
Pr_2NiO_4-$La_{10}Si_6O_{27}$	R-P		0.9 (850°C)	
$La_{0.6}Sr_{0.4}Fe_{0.8}Co_{0.2}O_3$-SDC	P	$La_{9.67}Si_{5.7}Mg_{0.3}O_{26.4}$	0.9 (700°C)	37
$La_{0.6}Sr_{0.4}Fe_{0.8}Co_{0.2}O_3$	P	$La_9SrSi_6O_{26.5}$	5.5-6.4 (700°C)	38
La_2NiO_4	R-P		0.8-1.7 (700°C)	
Pr_2NiO_4	R-P		0.2 (700°C)	
Nd_2NiO_4	R-P		0.7-0.3 (700°C)	
$(La_{0.74}Bi_{0.1}Sr_{0.16})MnO_3$	P	$La_{9.67}Si_{6-x}Al_xO_{26.5-x/2}$	0.81 (850°C)	39
$La_{0.8}Sr_{0.2}MnO_3$	P	$La_{10}Si_{5.5}Al_{0.5}O_{26.75}$	5.9	40
$La_{0.7}Sr_{0.3}FeO_3$	P		0.9	
$La_{0.6}Sr_{0.4}Fe_{0.8}Co_{0.2}O_3$	P		0.4	
$La_{0.6}Sr_{0.4}Fe_{0.2}Co_{0.8}O_3$	P		0.1	
$La_{0.75}Sr_{0.25}Cr_{0.5}Mn_{0.5}O_3$	P		3.3	
$La_{0.8}Sr_{0.2}MnO_3$	P	$La_9SrSi_6O_{26.5}$	2.3	41
$La_{0.6}Sr_{0.4}Co_{0.8}Fe_{0.2}O_3$	P		0.6	
$La_{0.6}Sr_{0.4}Co_{0.8}Fe_{0.2}O_3$-CGO	P		0.1	

Experimental

Synthesis of the oxides and preparation of pellets and symmetrical cells

Perovskite compounds were synthesised by solid state reaction from high purity commercial reagents: La_2O_3 (Sigma Aldrich, 99.99%), MnO (Sigma Aldrich, 99%), NiO (Alfa Aesar, 99%), Fe_2O_3 (Sigma Aldrich, >99%), Cr_2O_3 (Alfa Aesar, 98+%) and CuO (Sigma Aldrich, 99%). La_2O_3 was pre-heated at 980°C for 2 hours in order to achieve full decarbonation of the powder. Stoichiometric quantities of each oxide were mixed and heated at 1250°C for 12 hours, then ground again and reheated. In order to obtain dense pellets for electrical measurements, 1g of each compound was mixed with 10 drops of a 5%wt polyvinyl alcohol (Sigma Aldrich, 99+%) solution in water acting as a binder and ground until homogeneity. Then, cylindrical pellets of the compounds (~13 mm diameter and ~2 mm thickness) were made by uniaxial pressing, applying 490 MPa for 5 minutes. Different sintering temperatures (in the range of 1300°C and 1450°C) were applied for each compound in order to achieve suitable density. The relative density of the sintered pellets lies within the range of 65 to 80%.

Table 2. Compositions studied in this work for cathode applications

Cu^{2+} substitution	Ni^{2+} substitution
$LaMn_{0.8}Cu_{0.2}O_{3-\delta}$ — LM8C	$LaMn_{0.8}Ni_{0.2}O_{3-\delta}$ — LM8N
$LaMn_{0.7}Cu_{0.3}O_{3-\delta}$ — LM7C	$LaMn_{0.7}Ni_{0.3}O_{3-\delta}$ — LM7N
$LaFe_{0.8}Cu_{0.2}O_{3-\delta}$ — LFC	$LaFe_{0.8}Ni_{0.2}O_{3-\delta}$ — LFN
$LaCr_{0.8}Cu_{0.2}O_{3-\delta}$ — LCC	$LaCr_{0.8}Ni_{0.2}O_{3-\delta}$ — LCN

Apatite powder LSAO was also synthesised by solid state reaction adding two intermediate attrition milling steps. La_2O_3 (Sigma Aldrich, 99.99%), SiO_2 (Alfa Aesar, 99.8%), both decarbonised at 980°C for 2h, and Al_2O_3 (Sigma Aldrich, 99.99%) were mixed in an agate mortar. The mixture was attrition milled at 1500 rpm for 1 hour by means of a Eurostar Power-B IKA-Werke overhead stirrer. Once dried at 70°C overnight, the oxides mixture was pressed into disks as described before and heated at 1500°C for 4 hours, then ground and reheated. A second attrition milling step was applied to this powder, which allowed a better sintered pellet to be obtained. The sintering cycle consists of two successive steps, first at 1400°C for 2 hours and then at 1600°C for another 2 hours, using sacrificial powder of the same composition on top of the pellet in the furnace. Sintered apatite pellets had a relative density above 95%, in accordance with the requirement to work as an electrolyte in a solid oxide fuel cell.

Cathode deposition over the electrolyte was made through dip-coating of the sintered apatite pellet into a ceramic slurry of each cathode compound. To make these slurries, attrition milling was performed at 1500 rpm for 4 hours over the synthesized perovskite powders in order to reduce their particle size, thus leading to more stable suspensions. Beycostat C-213 dispersant (Stepan) was added to a mixture of perovskite and ethanol (45:55%wt.), stirring the mixture for homogeneity before the addition of polyvinyl butyral (Butvar B-76, Solutia) as a binder. Electrolyte pellets with a surface of approximately 0.25 cm^2 and 0.1 cm thickness were dip-coated in the prepared ceramic slurries, with 4 immersions of the pellet at a withdrawal speed of 3 mm/s. The as-prepared symmetrical cells were then sintered at 1000°C for 1 hour, with a slow heating rate (2°C/min) to avoid delamination of the cathode layer.

Characterization techniques

X-ray diffraction (XRD) measurements were carried out with a D/max 2500 RIGAKU diffractometer at 40 kV and 80 mA with a Cu-anode and a graphite monochromator to select Cu Kα radiation. Signal was recorded in the 10°-60° 2θ range with a step size of 0.03° and 1s per step. Raman spectroscopy was carried out using a backscattering geometry, with an optical microprobe spectrometer (Model XY, Dilor, France), a CCD Detector, a x50 microscope objective and the 496.5 nm line of an Ar^+-ion laser (INNOVA 200, Coherent, Palo Alto, CA) at a power of 25 mW. Microstructural characterization was performed by means of field emission scanning electron microscopy (FESEM) with a Carl Zeiss MERLIN microscope working at 15 kV and 218 pA.

Thermal expansion coefficients of the studied materials were measured using a Setsys Evolution 16/18 dilatometer (Setaram Instrumentation, KEP Technologies). Sintered samples were heated up to 1000°C for 0.5 hours and then the change in size was measured during the cooling ramp at a rate of 5°C/min. The measurements were made in a synthetic air atmosphere.

Electrochemical impedance spectroscopy (EIS) was used to determine the conductivity of the individual sintered compounds and the area-specific resistance (ASR) of the perovskite-apatite symmetrical cells. A frequency response analyser SI 1260 Schlumberger was used to perform the measurements. Pellets of the different compounds were painted beforehand with platinum ink (A4338A Metalor) and cured at 900°C for 4 hours. For the cathode pellets, four-point probe measurements were performed to get rid of the influence of platinum wires and contacts on the overall measured resistance. The conductivity of the materials was obtained from impedance measurements of pellet samples under zero DC bias, measuring up to 850°C from 0.1 Hz to 1 MHz and 50 mV AC voltage amplitude. Cathode resistance in symmetrical cells was obtained from EIS measurements in the 700-850°C IT-range from 0.1 Hz to 10 kHz, with an AC amplitude between 0.2 to 1 mA. Applied DC bias values varied between 0 and 40 $mA \cdot cm^{-2}$.

Results and Discussion

Synthesis, sintering and structural characterization

The XRD patterns of the single phases (powder and pellets) were compared with those compiled in the ICSD database[46] to look for secondary phases or unreacted reagents.

All the cathode materials were obtained as a single phase after the second treatment at 1250°C, as shown in fig. 1 (a). Conversely, after the first heating step there usually were observed small quantities of unreacted La_2O_3 in LM7N and LM8N, as well as NiO in LFN and LCN. A secondary phase of La_2CuO_4 was only found for LCC and LFC, but it disappeared upon grinding and reheating. Regarding the sintering, iron compounds needed temperatures as low as 1300°C to reach 75-80% relative density, while LCN and LM7N needed up to 1450°C to achieve densification. Sintering temperatures and obtained relative densities are shown in table 3. Despite firing at these temperatures, no decomposition or secondary phase formation could be found in the diffraction patterns of the pellets, as seen in fig. 1 (b).

Electrolyte powder and pellets were also characterized by means of X-ray diffraction and by Raman spectroscopy. Several approaches of solid-state synthesis were taken due to the difficulty to obtain dense enough pellets. By applying attrition milling, heating and reheating at 1500°C for 4 hours and another attrition milling step previous to the sintering step, no secondary phases could be identified at the XRD patterns, as can be seen in fig. 2 (a). In order to reach relative densities above 95%, a two-step sintering cycle was applied as described in the experimental section.

Profile matching of X-ray diffractograms was performed using Fullprof software.[47] The crystal structure and cell parameters obtained for each compound are given in table 4. The synthesised perovskite samples were indexed as orthorhombic with Pbnm symmetry, in good agreement with the literature.[48–53] The same procedure was carried out for LSAO apatite powders. Diffraction peaks were indexed with a hexagonal crystal structure with a P63 space group, as reported.[54] No decomposition or phase change into other structures was found upon sintering.

Table 3. Sintering temperature and relative densities of pellets of the synthesised compounds

Sample	T_{sint} (°C/h)	Relative density (%)
LCC	1400°C/8h	65
LCN	1450°C/4h	70
LFC	1300°C/4h	81
LFN	1300°C/4h	76
LM7C	1400°C/8h	65
LM7N	1450°C/4h	78
LM8C	1400°C/8h	70
LM8N	1400°C/8h	65
LSAO	1600°C/2h	97

Raman spectroscopy was used to look for any local changes in the LSAO pellets that could be detrimental to conductivity. A typical spectrum is given in fig. 2(b). All the observed bands agree with those reported in literature[55,56] and no segregations were found. The AlO_4 stretching vibration υ1 is observed as a weak peak at 730 cm^{-1}, consistent with the aforementioned literature.

Thermomechanical compatibility

The average thermal expansion coefficients (TEC) of the studied compounds were calculated by the following relation (1), in which L_0 is the length of the prism-shaped sample and ΔL and ΔT are the change in length and temperature, respectively.

$$\bar{\alpha} = -\frac{1}{L_0} \cdot \left(\frac{\Delta L}{\Delta T}\right) \qquad (1)$$

A similar behaviour was found for all the studied perovskite compounds. The slope of the $\Delta L/L_0$ curve shows a monotonous increase at low and high temperatures. At an intermediate temperature, different for each compound, a decrease in slope is observed (see fig. 3), although the study of this behaviour is out of the scope of this work. The thermal expansion values summarized in table 5 are averages in the temperature ranges indicated on the table.

The obtained TEC (from 623 to 1273 K) for LSAO apatite ($9.8 \cdot 10^{-6}$ K^{-1}) agrees with the values reported by Shaula et al., $9.92 \cdot 10^{-6}$ K^{-1},[15] and by Zhou et al., $9.73 \cdot 10^{-6}$ K^{-1}.[39]

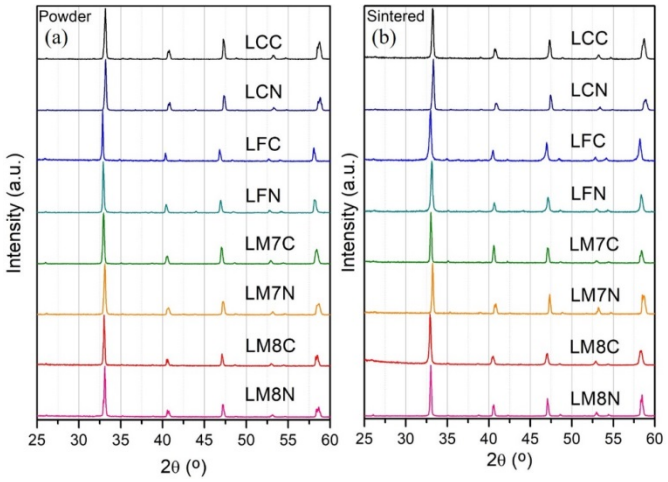

Figure 1. Selected region of XRD patterns for reheated perovskite powders at 1250°C/12h (a) and pellets of those compounds sintered at different temperatures (b).

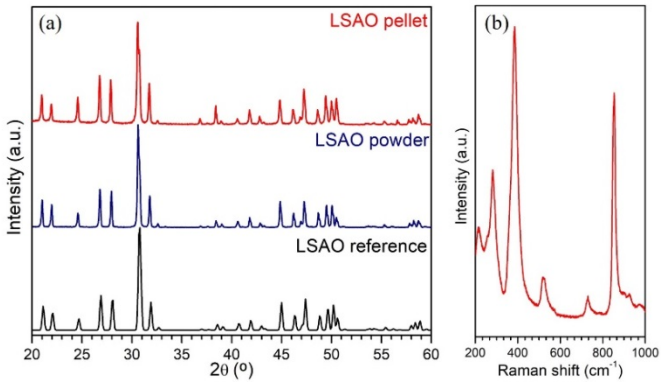

Figure 2. Structural characterization of the apatite electrolyte, (a) XRD for the reheated powder at 1500°C/4h and (b) Raman spectrum for the LSAO two-step sintered pellet at 1400°C/2h and 1600°C/2h.

Regarding the perovskite samples, manganite-derived perovskites show higher TECs than ferrite and chromite ones, both with nickel and copper substitution. Nevertheless, none of the compounds (except LM8C) exceeded $12.5 \cdot 10^{-6}$ K^{-1} and this difference with the apatite TEC in this temperature range is tolerable for the compounds to act as electrodes.

Table 4. Synthesised cathode and electrolyte powders, crystal structure and lattice parameters

Sample	Crystal system	Space group	Lattice parameters a (Å)	b (Å)	c(Å)	Cell volume V/Z (Å³)
LCC	orthorhombic	P b n m	5.5166(2)	5.4866(2)	7.7664(4)	235.07(2)
LCN	orthorhombic	P b n m	5.5100(4)	5.4743(5)	7.7524(7)	233.84(4)
LFC	orthorhombic	P b n m	5.406(1)	5.5461(1)	7.8458(3)	235.24(4)
LFN	orthorhombic	P b n m	5.5457(9)	5.5423(7)	7.831(1)	240.69(6)
LM7C	orthorhombic	P b n m	5.5390(1)	5.5098(1)	7.8093(2)	238.33(1)
LM7N	orthorhombic	P b n m	5.5191(7)	5.4843(8)	7.771(1)	235.20(1)
LM8C	orthorhombic	P b n m	5.5328(3)	5.5096(3)	7.7921(6)	237.53(3)
LM8N	orthorhombic	P b n m	5.5231(5)	5.4777(8)	7.769(1)	235.04(5)
LSAO	hexagonal	P 63	9.7196(2)	9.7196(2)	7.2112(2)	590.18(1)

Chemical compatibility

In order to test whether a reaction between the electrolyte and cathode materials might take place either at operating or sintering temperatures, the same amounts of perovskite and apatite powders were mixed thoroughly and subjected to thermal treatments. The mixtures were heated at two temperatures for 12 hours, 900°C and 1250°C, one slightly above the operational temperature of the IT-SOFC and the other one above the sintering temperature.

In fig. 4, XRD patterns of nickel-substituted compounds treated at 900°C (a) and 1250°C (b) and copper-substituted compounds at 900°C (c) and 1250°C (d) are shown. Neither secondary phases nor decomposition of the original apatite and perovskites could be found in any of the diffractograms, so no reaction had taken place between apatite and perovskite even at temperatures higher than the possible sintering temperature, proving that these materials are chemically compatible and could therefore be used together in a SOFC.

Electrical conductivity

Pellets of LSAO were prepared as described in the experimental section, to be used as support electrolytes to prepare symmetrical cells. First, their conductivity was determined by electrochemical impedance spectroscopy (EIS) using Pt-paste electrodes on 97% dense pellets.

Nyquist plots had the usual shape, as shown in fig. 5, which corresponds to the measurement at around 600°C of the sintered apatite. Nyquist plots showed a low frequency arc associated with the electrodes and two depressed arcs at higher frequencies. Their equivalent capacitances indicated that they were associated with bulk conduction (at the highest frequencies) and grain boundary (medium frequencies). Of course, not all contributions could be measured at all temperatures, as the respective frequencies shifted towards higher values as the temperature was raised, eventually lying out of the equipment measuring range. Our interest here was to identify appropriate synthesis and sintering conditions that would generate a good conducting electrolyte to test against the perovskite electrodes. Therefore, only the total conductivity (σ) of the electrolyte is shown on the inset of fig.5, in an Arrhenius plot, obtained using the following relations (2) and (3).

$$\sigma = \frac{1}{R} \cdot \frac{l}{S} \qquad (2)$$

$$\sigma = \frac{A}{T} \cdot e^{-\left(E_a / k \cdot T\right)} \qquad (3)$$

Where l and S are the thickness and surface of the pellet, respectively, R is the measured resistance of the electrolyte, A is the pre-exponential factor, E_a is the activation energy and k is the Boltzmann constant. The total conductivity of the apatite is $9.4 \cdot 10^{-3}$ S·cm^{-1} at 800°C and $4.9 \cdot 10^{-3}$ S·cm^{-1} at 700°C, in agreement with previous works,[11] while other authors reported lower values.[54] The activation energy is obtained from the linear fitting of ln(σ·T) vs 1/T, according to expression (3), where E_a is 0.67 eV in the 550-850°C temperature range. These values make LSAO suitable for its use as an electrolyte for IT-SOFC.

Table 5. Average thermal expansion coefficients for the sintered perovskites and apatite in the indicated temperature range of the dilatometric cycle, measured while cooling the sample

Sample	ᾱ (K^{-1}) (RT to 1273 K)	ᾱ (K^{-1}) (623 to 1273 K)
LCC	$8.7 \cdot 10^{-6}$	$10.2 \cdot 10^{-6}$
LCN	$9.5 \cdot 10^{-6}$	$11.0 \cdot 10^{-6}$
LFC	$11.0 \cdot 10^{-6}$	$11.7 \cdot 10^{-6}$
LFN	$11.5 \cdot 10^{-6}$	$12.2 \cdot 10^{-6}$
LM7C	$10.0 \cdot 10^{-6}$	$12.5 \cdot 10^{-6}$
LM7N	$10.1 \cdot 10^{-6}$	$12.0 \cdot 10^{-6}$
LM8C	$11.1 \cdot 10^{-6}$	$12.1 \cdot 10^{-6}$ (623-973 K) $15.5 \cdot 10^{-6}$ (973-1273 K)
LM8N	$9.9 \cdot 10^{-6}$	$11.4 \cdot 10^{-6}$
LSAO	$9.1 \cdot 10^{-6}$	$9.8 \cdot 10^{-6}$

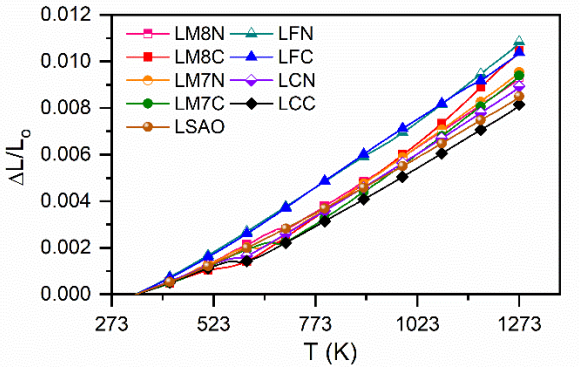

Figure 3. Thermal expansion of the materials from 1000°C to RT.

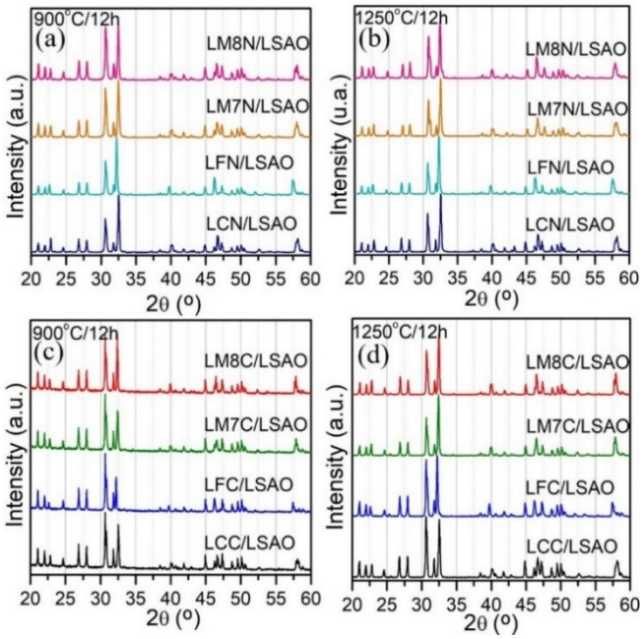

Figure 4. X-ray diffractograms for a 1:1 weight mixture of apatite with nickel-substituted perovskites heated at (a) 900°C for 12 hours and (b) 1250°C for 12 hours and with copper-substituted perovskites heated at (c) 900°C for 12 hours and (d) 1250°C for 12 hours.

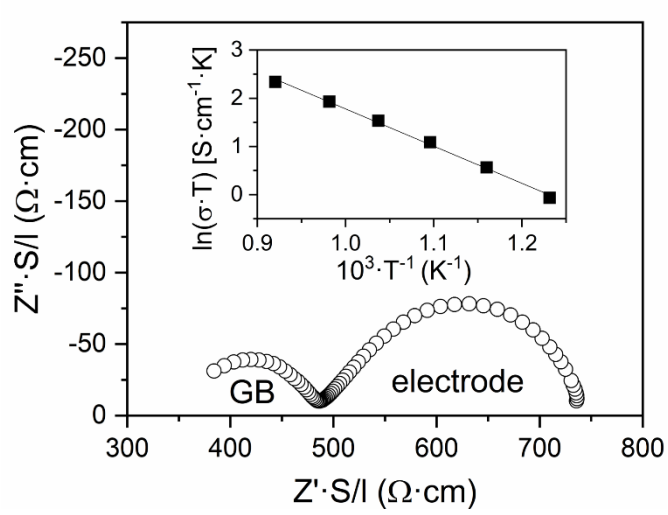

Figure 5. Nyquist plot for the EIS measurement of the LSAO apatite with a platinum electrode at 589°C, showing low frequency (electrode) and medium frequency (grain boundary, GB) arcs. On the inset, the Arrhenius plot for the total conductivity of LSAO.

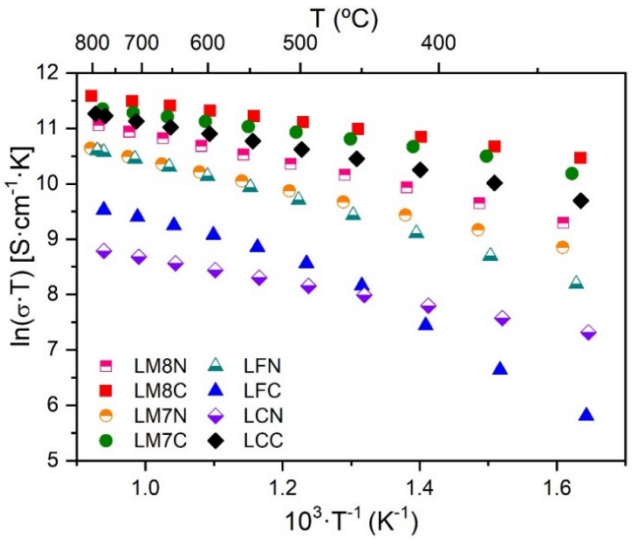

Figure 6. Arrhenius plot for the electrical conductivity of the different sintered perovskites.

Regarding the perovskite electrical conductivities, it has been previously reported that these materials follow a small polaron hopping electronic conduction mechanism.[29,42,43] The resistance of the perovskite pellets was measured with a 4-point probe set-up. Fig. 6 shows the Arrhenius plot for the calculated conductivities in the whole temperature range. The conductivity of every compound follows a linear trend except LFN and LFC, especially the last one.

The conductivity of the ferrites shows an abrupt change in activation energy around 500°C. It has been reported for $LaFe_{0.8}Cu_{0.2}O_{3-\delta}$ that both Fe^{3+} and Fe^{4+} coexist at the perovskite B-sites,[44] and thus the oxidation states of Cu and Ni could also change with temperature. This change might be a possible explanation for the abrupt enhancement of conductivity and for LFN and LFC not following the same temperature dependence as the other perovskites in the 300-500°C temperature range.

As seen in table 6, conductivity values at 800°C vary between 10-100 S·cm^{-1}, which means all the compounds show a similar behaviour, adequate for their use as electrodes. Manganese-copper compounds show the highest electronic conductivities at 800°C, being 80 S·cm^{-1} for LM7C and almost 100 S·cm^{-1} for LM8C and they also offer the lowest activation energies (0.13 eV). When substituting manganites with nickel, lower electronic conductivities (~40 and 60 S·cm^{-1} for LM7N and LM8N, respectively) and higher activation energies (0.22 eV) in the high temperature range are found. Chromium compounds show the same activation energies (0.18 eV), but very different conductivities at 800°C, with LCC showing a value of above 70 S·cm^{-1} and LCN as low as 6 S·cm^{-1}. Substituted iron-based compounds show intermediate values of conductivity at that temperature (14 S·cm^{-1} for LFC and 40 S·cm^{-1} for LFN), but their activation energy of 0.28 eV, the same for both of them, is the highest for the eight studied compounds. It must be noted that since the relative density values for the perovskite pellets vary between 65 and 80% of their theoretical density, conductivity values for each compound might be up to 2 times the measured values.

The obtained values are comparable to those of some cathode materials found in the literature, although these values are strongly dependent on the pellet characteristics. Manganese-nickel perovskite compounds behave as reported,[42] with LM8N being more conductive than LM7N and the latter having a higher activation energy than the former. The same behaviour is found for LM8C, which is more conductive than LM7C. Therefore, it can be concluded that for these compositions, higher amounts of copper or nickel tend to diminish the electronic conductivity of the compounds in this range of compositions.

The LFN conductivity at 800°C is 38.3 S·cm^{-1}, very close to the 22 S·cm^{-1} also reported,[42] and the value obtained for LCN, 6.2 S·cm^{-1}, is practically identical to the previously reported value of 8.2 S·cm^{-1}.[29] For the copper compounds there are not many reported values, although the LFC value of 13.6 S·cm^{-1} differs from the 42 S·cm^{-1} found for the same composition.[44]

Table 6. Summary of the electrical conductivities of the compounds at 800°C and the activation energies in the 400-800°C range, except for LFC and LFN, given in the 500-800°C range

Sample	σ at 800°C (S·cm^{-1})	E_a (eV)
LCC	72.5	0.180
LCN	6.2	0.180
LFC	13.6	0.279
LFN	38.3	0.282
LM7C	80.0	0.130
LM7N	37.6	0.226
LM8C	98.6	0.133
LM8N	59.3	0.217

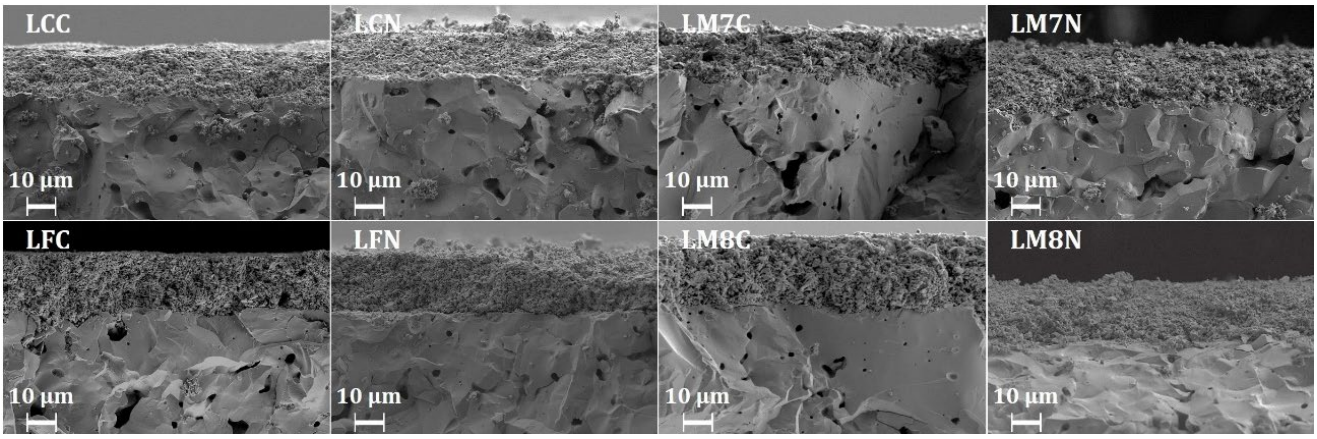

Figure 7. SEM micrographs of the fractured cross-section of the symmetrical cells at 1000x. The lower part of the images shows the dense LSAO electrolyte, the upper part corresponds to the respective porous electrode material as indicated in the lettering.

Symmetrical cell microstructure and ASR measurements

As-prepared perovskite powders led to low stability ceramic suspensions due to their grain size and morphology. Thus, an attrition-milling step was needed as described before, and afterwards most of the particles were about 1.5 µm in size, leading to more stable suspensions.

The sintered dip-coated electrodes show good adherence with the electrolyte (see fig. 7). Their thickness stays in the range from 15 to 25 µm, and average thickness values for each compound are given in table 7. The electrodes are porous and they all have grains of around 1 µm, with different proportions of smaller particles (down to 100 to 200 nm). In general, the manganese-containing compounds show larger particles.

The resistance measurements were performed in air atmosphere via EIS in the intermediate-temperature range and the values of the electrodes area-specific resistance were calculated from the relation (4) where Rp is the polarization resistance of the electrode contribution to the impedance and S is the single electrode surface.

$$\mathrm{ASR} = \mathrm{R_p} \cdot \frac{\mathrm{S}}{2} \qquad (4)$$

The Nyquist plot for the LFC_LSAO symmetrical cell is shown in fig. 8 for 735, 785 and 840°C. Ohmic resistance corresponding to the electrolyte has been subtracted for all three arcs for a better visualization of the polarization resistance of the electrodes at different temperatures.

The obtained electrode ASR values are shown in fig. 9. The electrode resistance decreases logarithmically with temperature, which means that this process is thermally activated. The slopes of the ASR vs. 1/T plots give activation energies between 1 and 1.8 eV. ASR values at 700°C are summarized in table 5. In general, copper-substituted compounds exhibit smaller polarization resistance than their nickel analogues, whose ASR values lie approximately between 50 and 200 Ω·cm^2 at 700°C.

LFC stands out among the rest of the perovskite compositions. Idrees et al.[44] also found low ASRs for this compound as electrode on samarium doped ceria electrolyte. Its area-specific resistance of 4,3 Ω·cm^2 at 700°C is comparable to other perovskite compositions tested as cathodes with an apatite electrolyte. The amount of references in which such a cell is studied is scarce. LSM on a $La_{10}Si_{5.5}Al_{0.5}O_{26.75}$ electrolyte showed 50 Ω·cm^2 at 700°C,[40] and a composite of LSM:40%wt.CGO on $La_{10}Si_5AlO_{26.5}$ gave a similar value of 33.4 Ω·cm^2 at the same temperature.[32] It was found that using a strontium-doped apatite like $La_9SrSi_6O_{26.5}$ (LSSO), LSM had an area-specific resistance of just 13 Ω·cm^2.[41] A $La_{0.6}Sr_{0.4}Fe_{0.8}Co_{0.2}O_{3-\delta}$ (LSCF) perovskite cathode was tested also on LSSO, giving rise to a value of 5.5 Ω·cm^2 at 700°C,[38] while an iron-nickel cathode LSFN was tested on $La_{9.83}Si_5Al_{0.75}Fe_{0.25}O_{26}$ and its ASR was 65 Ω·cm^2 at 700°C.[35] All these values are noticeably higher than the one found for LFC in this study. Thus, it can be concluded that performance of LFC as a cathode with an LSAO apatite electrolyte is comparable to the best results obtained so far. It is worth pointing out that, as these are mainly electronic conductors, the performance of composite apatite-perovskite electrodes is expected to improve that of single phase electrodes.

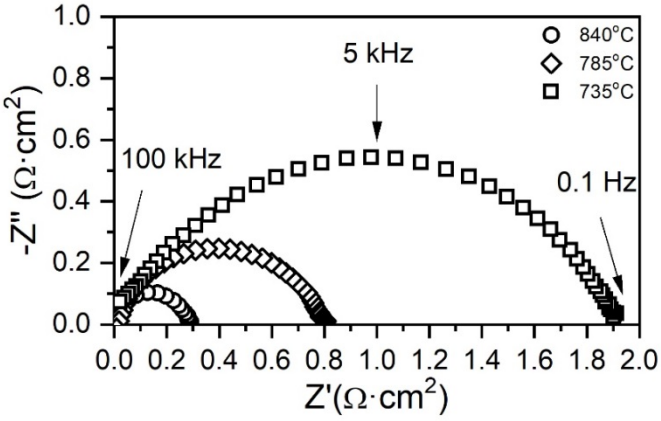

Figure 8. Nyquist plot for the LFC electrodes on LSAO electrolyte at different temperatures and frequencies. Z' and Z'' values have been scaled to the surface of the LFC electrode. The measurements were done in an air atmosphere.

Table 7. Electrode area-specific resistances at 700°C of the perovskite-apatite symmetrical cells sintered at 1000°C/1h with zero DC bias and with 8 mA·cm^{-2} DC bias

Half cell	Electrode thickness (μm)	ASR at 700°C (Ω·cm^2)	
		Zero DC bias	I_{DC} = 8 mA·cm^{-2}
LCC_LSAO	18.9 ± 3.0	32	13
LCN_LSAO	14.1 ± 1.9	52	9.3
LFC_LSAO	19.0 ± 1.9	4.3	3.0
LFN_LSAO	18.5 ± 2.2	102	9.0
LM7C_LSAO	15.4 ± 1.5	150	9.5
LM7N_LSAO	19.3 ± 2.1	206	17
LM8C_LSAO	24.7 ± 3.4	90	7.9
LM8N_LSAO	22.5 ± 2.8	182	20

The rest of the compounds exhibit more resistive behaviour than that of LFC and the only ones that show a resistance similar to some of the values found in the literature are the chromium compounds LCC and LCN with 32 and 52 Ω·cm^2 at 700°C, respectively. On the other hand, manganese-nickel compounds, LM7N and LM8N, show the largest area-specific resistances of all the studied compounds. It has been suggested that manganese compounds might lead to some interfacial reaction with the apatite electrolyte,[40] but that explanation does not seem to fit in this particular case, since EDS analysis did not show any cation interdiffusion or reactivity between cathode and electrolyte components.

Applying DC bias to the symmetrical cells did not affect the ohmic resistance of the electrolyte in this range of temperatures, but it made the polarization resistance of the electrodes decrease in the 700-850°C temperature range. This might be indicative of oxygen exchange reaction being rate limiting in the performance of these compounds as electrodes.[57] This is to be expected with electrodes which are mainly electronic conductors. Electrode area-specific resistances of the cells under 8 mA·cm^2 DC bias are shown in fig. 10.

This small current density activated the electrodes, such that all compounds gave electrode ASR values of around 10 Ω·cm^2. Little to no dependence of the area-specific resistance with temperature remains in this temperature range, suggestive of a change of the rate limiting process. LFC does not follow this trend, but requires higher DC current densities to reduce its ASR in this temperature range. Area-specific resistances of the electrodes at 700°C when applying DC bias are summarized in table 7.

Conclusions

A series of strontium and cobalt-free perovskite compounds have been investigated as suitable candidates to work as cathodes on an IT-SOFC design with an aluminium-doped lanthanum silicate apatite (LSAO) as electrolyte.

All compounds have been successfully synthesised, as no secondary phase could be detected by means of x-ray diffraction, neither in the as-prepared powder nor in the sintered pellets manufactured at high temperature. The chemical compatibility with LSAO was verified by XRD on mixtures of the powdered compounds after high temperature treatments, as well as by EDS across the interphases of sintered half cells. The thermomechanical compatibility between LSAO and the studied compounds was also proven, since there are no great differences in the thermal expansion of electrode and electrolyte materials in a wide range of temperatures.

Regarding their functional characterization, the electrical conductivity of the different perovskite materials varied from ~10 to 100 S·cm^{-1} at 800°C, with manganese-copper compounds LM7C and LM8C being the ones with higher conductivities and lower activation energies.

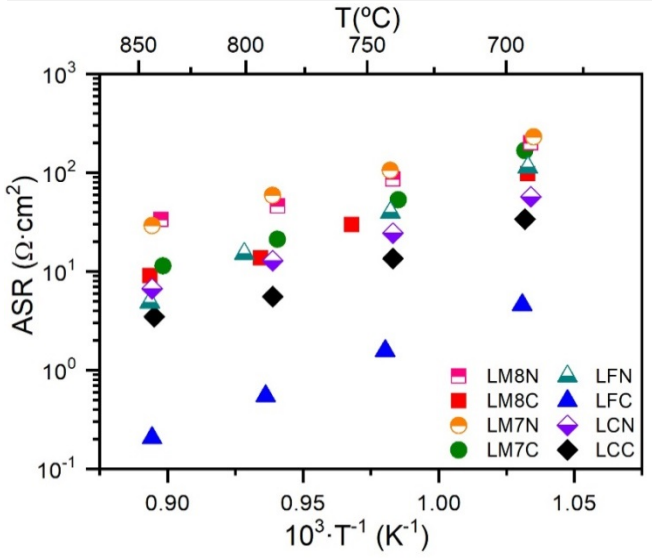

Figure 9. Area-specific resistance of the perovskite electrodes deposited on the LSAO apatite pellet.

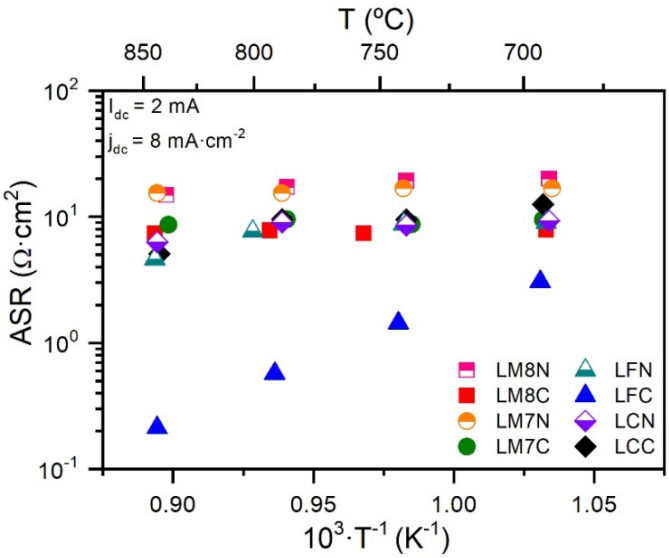

Figure 10. Area-specific resistance of the electrodes when applying 8 mA·cm^{-2} DC bias.

The area-specific resistance of the perovskite electrodes in symmetrical cell configuration with the apatite electrolyte was measured. Copper compounds showed lower ASR values than their nickel analogues, with LFC being the most promising material to work alongside the apatite electrolyte, with its ASR value of 4.3 Ω·cm^2 at 700°C comparable to those obtained for traditional LSM cathodes. Moreover, the application of small DC bias has been shown to decrease largely the activation energy of the electrodes with higher polarization resistance. Since the electrochemical response of these perovskite compounds as oxygen electrodes on LSAO is encouraging, the performance of the cells would benefit from further optimization of the perovskite powder, cell microstructure and apatite/perovskite interface.

Conflicts of interest

There are no conflicts to declare.

Acknowledgements

This work was financially supported by Spanish Government MAT2015-68078-R (MINECO/FEDER, UE) and RTI2018-098944-J-I00 (MCIU/AEI/FEDER, UE) grants and BES-2016-078508 FPI grant and a flexifund grant under the EPSRC EP/R023662/1 JUICED project, which allowed the author to perform initial experiments at the University of Birmingham under the supervision of Prof. Peter R. Slater. Authors would like to acknowledge the use of Servicio General de Apoyo a la Investigación-SAI, Universidad de Zaragoza.

Notes and references

1 A. Orera and P. R. Slater, *Chem. Mater.*, 2010, **22**, 675–690.
2 N. Mahato, A. Banerjee, A. Gupta, S. Omar and K. Balani, *Prog. Mater. Sci.*, 2015, **72**, 141–337.
3 S. Nakayama, T. Kageyama, H. Aono and Y. Sadaoka, *J. Mater. Chem.*, 1995, **5 (11)**, 1801–1805.
4 S. Nakayama and M. Sakamoto, *J. Eur. Ceram. Soc.*, 1998, **18**, 1413–1418.
5 S. Célérier, C. Laberty, F. Ansart, P. Lenormand and P. Stevens, *Ceram. Int.*, 2006, **32**, 271–276.
6 J. R. Tolchard, M. S. Islam and P. R. Slater, *J. Mater. Chem.*, 2003, **13**, 1956–1961.
7 K. Kobayashi, K. Hirai, T. S. Suzuki, T. Uchikoshi, T. Akashi and Y. Sakka, *J. Ceram. Soc. Japan*, 2015, **123 (4)**, 274–279.
8 A. Najib, J. E. H. Sansom, J. R. Tolchard, P. R. Slater and M. S. Islam, *Dalt. Trans.*, 2004, **19**, 3106–3109.
9 J. E. H. Sansom, E. Kendrick, J. R. Tolchard, M. S. Islam and P. R. Slater, *J. Solid State Electrochem.*, 2006, **10**, 562–568.
10 H. Yoshioka, Y. Nojiri and S. Tanase, *Solid State Ionics*, 2008, **179**, 2165–2169.
11 L. Dai, W. Han, Y. Li and L. Wang, *Int. J. Hydrogen Energy*, 2016, **41**, 11340–11350.
12 S. Beaudet-Savignat, A. Vincent, S. Lambert and F. Gervais, *J. Mater. Chem.*, 2007, **17**, 2078–2087.
13 H. Yoshioka, *J. Am. Ceram. Soc.*, 2007, **90 (10)**, 3099–3105.
14 L. León-Reina, J. M. Porras-Vázquez, E. R. Losilla and M. A. G. Aranda, *Solid State Ionics*, 2006, **177**, 1307–1315.
15 A. L. Shaula, V. V. Kharton and F. M. B. Marques, *J. Solid State Chem.*, 2005, **178**, 2050–2061.
16 Y. Chen, W. Zhou, D. Ding, M. Liu, F. Ciucci, M. Tade and Z. Shao, *Adv. Energy Mater.*, 2015, **5**, 1–34.
17 S. P. Jiang, *J. Mater. Sci.*, 2008, **43**, 6799–6833.
18 W. Wang and S. P. Jiang, *Solid State Ionics*, 2006, **177**, 1361–1369.
19 Y. Li, W. Zhang, Y. Zheng, J. Chen, B. Yu, Y. Chen and M. Liu, *Chem. Soc. Rev.*, 2017, **46**, 6345–6378.
20 W. Jung and H. L. Tuller, *Energy Environ. Sci.*, 2012, **5**, 5370–5378.
21 H. Dulli, P. Dowben, S.-H. Liou and E. W. Plummer, *Phys. Rev. B*, 2000, **62 (22)**, 629–632.
22 T. T. Fister, D. D. Fong, J. A. Eastman, P. M. Baldo, M. J. Highland, P. H. Fuoss, K. R. Balasubramaniam, J. C. Meador and P. A. Salvador, *Appl. Phys. Lett.*, 2008, **93**, 1–3.
23 Y. Chen, W. Jung, Z. Cai, J. J. Kim, H. L. Tuller and B. Yildiz, *Energy Environ. Sci.*, 2012, **5**, 7979–7988.
24 D. Oh, D. Gostovic and E. D. Wachsman, *J. Mater. Res.*, 2012, **27 (15)**, 1992–1999.
25 P. A. W. Van Der Heide, *Surf. Interface Anal.*, 2002, **33**, 414–425.
26 A. Weber and E. Ivers-Tiffée, *J. Power Sources*, 2004, **127**, 273–283.
27 N. A. Baharuddin, A. Muchtar and M. R. Somalu, *Int. J. Hydrogen Energy*, 2017, **42**, 9149–9155.
28 E. V. Tsipis and V. V. Kharton, *J. Solid State Electrochem.*, 2008, **12**, 1367–1391.
29 V. V. Kharton, A. A. Yaremchenko and E. N. Naumovich, *J. Solid State Electrochem.*, 1999, **3**, 303–326.
30 F. Zhao, R. Peng and C. Xia, *Mater. Res. Bull.*, 2008, **43**, 370–376.
31 A. A. Yaremchenko, V. V. Kharton, D. O. Bannikov, D. V. Znosak, J. R. Frade and V. A. Cherepanov, *Solid State Ionics*, 2009, **180**, 878–885.
32 E. V. Tsipis, V. V. Kharton and J. R. Frade, *Electrochim. Acta*, 2007, **52**, 4428–4435.
33 T. Mitsui, A. Mineshige, T. Funahashi, H. Mieda, Y. Daiko, M. Kobune, H. Yoshioka and T. Yazawa, *J. Power Sources*, 2012, **217**, 170–174.
34 C. Bonhomme, S. Beaudet-Savignat, T. Chartier, P. M. Geffroy and A. L. Sauvet, *J. Eur. Ceram. Soc.*, 2009, **29**, 1781–1788.
35 H. Gasparyan, C. Argirusis, C. Szepanski, G. Sourkounic, V. Stathopoulos, T. Kharlamova, V. Sadykov and S. Bebelis, *ECS Trans.*, 2009, **25 (2)**, 2681–2688.
36 P. Jena, P. K. Patro, A. Sinha, R. K. Lenka, A. K. Singh, T. Mahata and P. K. Sinha, *Energy Technol.*, 2018, **6**, 1739–1746.
37 Y. X. Liu, S. F. Wang, Y. F. Hsu and C. H. Wang, *J. Power Sources*, 2018, **381**, 101–106.
38 B. Philippeau, F. Mauvy, C. Mazataud, S. Fourcade and J.-C. Grenier, *Solid State Ionics*, 2013, **249–250**, 17–25.
39 J. Zhou, X. F. Ye, J. L. Li, S. R. Wang and T. L. Wen, *Solid State Ionics*, 2011, **201**, 81–86.
40 D. Marrero-López, M. C. Martín-Sedeño, J. Peña-Martínez, J. C. Ruiz-Morales, P. Núñez, M. A. G. Aranda and J. R. Ramos-Barrado, *J. Power Sources*, 2010, **195**, 2496–2506.
41 J. M. Porras-Vázquez, L. Dos Santos-Gómez, I. Santacruz, M. A. G. Aranda, D. Marrero-López and E. R. Losilla, *Ceram. Int.*, 2012, **38**, 3327–3335.
42 E. Niwa, H. Maeda, C. Uematsu and T. Hashimoto, *Mater. Res. Bull.*, 2015, **70**, 241–247.
43 R. Chiba, F. Yoshimura and Y. Sakurai, *Solid State Ionics*, 1999, **124**, 281–288.
44 A. Idrees, X. Jiang, G. Liu, H. Luo, G. Jia, Q. Zhang, L. Jiang, X. Li and B. Xu, *ChemistryOpen*, 2018, **7**, 688–695.
45 S. C. Singhal, *Solid State Ionics*, 2000, **135**, 305–313.

46 Inorganic Crystal Structure Database, FIZ Karlsruhe, https://icsd.fiz-karlsruhe.de/search/basic.xhtml (accessed October 2020).
47 J. Rodriguez-Carvajal, "FULLPROF: A Program for Rietveld Refinement and Pattern Matching Analysis", *Abstracts of the Satellite Meeting on Powder Diffraction of the XV Congress of the IUCr*, p. 127, Toulouse, France (1990).
48 I. Qasim, P. E. R. Blanchard, S. Liu, B. J. Kennedy and M. Avdeev, *Inorg. Chem.*, 2014, **53**, 2240–2247.
49 J. Yang, *Acta Crystallogr.*, 2008, **64**, 281–286.
50 T. Caronna, F. Fontana, I. N. Sora and R. Pelosato, *Mater. Chem. Phys.*, 2009, **116**, 645–648.
51 E. A. Kiselev, N. V. Proskurnina, V. I. Voronin and V. A. Cherepanov, *Inorg. Mater.*, 2007, **43**, 167–175.
52 A. N. Petrov, A. Y. Zuev, I. L. Tikchonova and V. I. Voronin, *Solid State Ionics*, 2000, **129**, 179–188.
53 J. Blasco, M. C. Sánchez, J. Pérez-Cacho, J. García, G. Subías and J. Campo, *J. Phys. Chem. Solids*, 2002, **63**, 781–792.
54 K. Ueda, *J. Ceram. Soc. Japan*, 2012, **120 [2]**, 74–76.
55 G. Lucazeau, N. Sergent, T. Pagnier, A. Shaula, V. Kharton and F. M. B. Marques, *J. Raman Spectrosc.*, 2007, **38**, 21–33.
56 A. Orera, E. Kendrick, D. C. Apperley, V. M. Orera and P. R. Slater, *Dalt. Trans.*, 2008, **39**, 5296–5301.
57 H. Zhao, F. Mauvy, C. Lalanne, J. M. Bassat, S. Fourcade and J. C. Grenier, *Solid State Ionics*, 2008, **179**, 2000–2005.